# Aquapiling: Coated Substrate-Related Influences on Reverse Piling from a One-Side Single Colour Image in Multicolour Offset Printing

Patrick A.C. Gane*[+], Cathy J. Ridgway*, Peter Burri*, Manfred Arnold*, Karl-Heinz Kagerer*, Barry Madden[#], Matti Ristolainen[#] and Jarkko Purontaus[#]

## Abstract

A series of 11 coated papers, ranging from single coated LWC to multicoated woodfree grades, was tested extensively on a heatset web offset press under chosen conditions shown to create problems of heavy build-up on the blanket occurring at the non-image area of a later unit on stochastic mid tone areas where no image existed on the reverse side - termed reverse piling. The nature of the deposit, and the fact that it corresponded to the one side image area only, led to hypothesise an interaction between the printed image on the coated paper and the fountain solution gaining access at each subsequent unit from both the reverse side and the black image side where no further colour was applied. Raising the temperature on the press by reducing fountain solution cooling made the phenomenon significantly worse when using an alcohol-free fountain solution. It is shown by using methods of permeability, porosimetry, ink tack development and coating structure network modelling, that the problem is linked to the combination of two main properties: low absorption potential by the basepaper matched by a lack of permeability of the coating when and only when a predominance of nanopores (< 0.1 μm) is present – a feature needed in modern press rooms for fast setting and the required speed of turn around of the printed product. The phenomenon of reverse piling in this case of fountain solution interaction is described using the novel term, "aquapiling".

[*]Research and Technology Services, Omya AG, CH-4665 Oftringen, Switzerland

[+] Professor of Printing Technology at the Helsinki University of Technology, Laboratory of Paper and Printing Technology, P.O. Box 6300, FI-02015 TKK, Finland

[#]UPM Research Center, UPM-Kymmene Corporation, FI-53200 Lappeenranta, Finland

**Keywords**: reverse piling, aquapiling, coating permeability, base paper absorption, ink-fountain interactions

## 1. Introduction

Blanket piling in the offset press is often related to the ink tack behaviour on paper, especially in relation to the relative adhesion between the blanket and the paper surface. In the case of coated papers, the tack increase as a function of time has frequently been implicated [Concannon and Wilson, 1992, Gane *et al*., 1994] as a cause of blanket piling. In parallel, the effect of fountain solution as the cause for water interference mottling and/or tail edge picking is often associated with an inability of a coated paper to remove fountain solution laid down on a previous unit before further ink is applied.

In the cases discussed here, the piling tendency of a series of 11 commercial papers was studied on a heatset web offset press, using an ink and fountain solution combination, which, together with the standard press settings, led in some cases to an extreme blanket build-up on a subsequent printing unit, usually the last colour unit, of the first laid-down colour. The effect was exacerbated when using high tack ink and an alcohol-free fountain solution, especially at high temperature, effected by reduced fountain solution cooling. The reverse piling effect was predominant in areas where the paper was only printed on one side by a single colour (stochastic mid tone black). The build-up was not seen as progressive along the unit train, but appeared suddenly at the last printing unit indicating that a threshold had been reached beyond which the adhesion of the ink to the coating surface failed and transfer occurred onto the printing blanket. Furthermore, the nature of the distribution of the deposit indicated a delocalisation of the ink once separated from the paper surface, i.e. a planar shearing of the ink laterally over the blanket, as shown in the photograph in Figure 1.

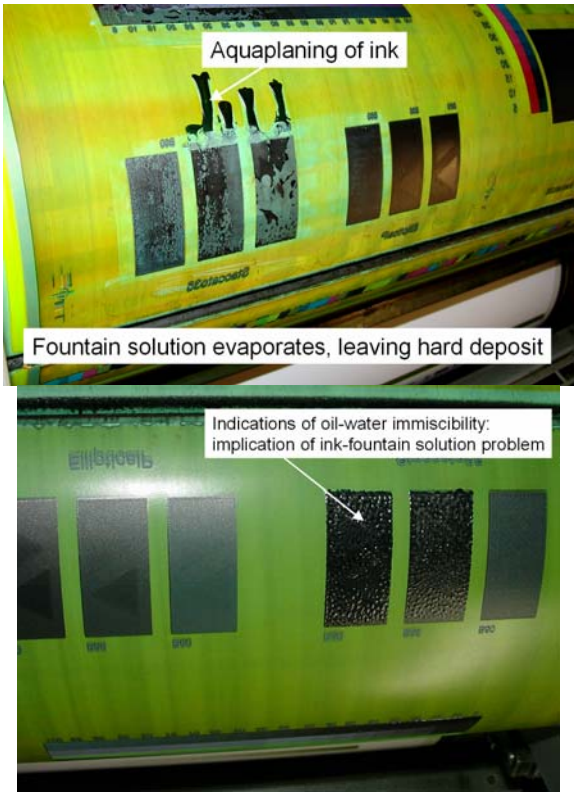


***Figure 1*** *The photographs show the reverse piling of the first laid black ink on the last unit (yellow) of the heatset press: indications of delocalisation of ink deposits and shearing by the proposed aquaplaning ("aquapiling") mechanism.*

No simple correlation could be found between the coating pigment formulation and the reverse piling tendency. This, even though the papers in question ranged from predominantly clay-containing light weight coatings on wood containing basepapers, through higher calcium carbonate-containing coatings on alkaline wood containing and woodfree light and medium weight coatings, respectively, to carbonate dominating heavy weight multicoated alkaline woodfree grades. The commercial papers used came from both North America and from Europe.

The threshold nature of the problem, i.e. its sudden appearance in the last printing unit, and the positioning of the adhesion failure to the paper coating surface, led to the hypothesis that a surfeit of fountain solution on or near the paper surface acting either to lift the ink from the surface by the action of film

continuity next to the blanket [Gane *et al*., 2000a], where the force to separate a thin film between two plane surfaces increases dramatically as a function of the separation and speed, or by the hydraulic pressure from under the ink as excess fountain solution is expelled at the surface under the pressure of the printing nip, a proposal made previously by Ridgway *et al.* [Ridgway *et al*., 2002] in the case of a newly developed light weight coated newsprint product. To test this hypothesis the interaction of liquid and substrate is studied together with the pore structure of the coatings.

A broad range of analyses has been applied, including the absorption of liquid by wicking into the *xy* planar direction of the paper (machine direction), air and liquid permeability of the coated sheet in the transplanar *z* direction, ink-on-paper tack development using the ISIT device [Gane *et al*., 1994], mercury intrusion porosimetry and subsequent modelling of the coating layer permeability using a network model Pore-Cor (a software package of the Environmental and Fluid Modelling Group, University of Plymouth, PL4 8AA, UK.).

## 1.1. Paper Samples and Ranked Performance

A summary of the 11 paper samples and their component analysis for this study is shown in Table 1. The ranking was made visually on the press in respect to the level of blanket build-up, together with tape-pull samples and photographs made after 35 000 - 40 000 copies. The printing plate used was half conventional screening and half stochastic. The greatest build-up occurred in the stochastic mid tone regions (20 %, 35 % and 50 %).

All pilot printing, four trials in all, were made at the Future Printing Center (FPC) in Raisio, Finland on a Heidelberg Web 8 with a cutting length of 630 mm and web width of 500 mm. Printing was done with both typical European printing conditions and typical N. American printing conditions with this equipment. The test conditions are summarised in Table 2.

The print layout (Figure 2) included both conventional and stochastic screening sections, the stochastic screening being used to represent the effect of finer dots in respect to their increased dot perimeter length, equivalent to 70 lines per inch. The web was divided into two conventional and two stochastic sectors in the machine direction. All the pictures and colour bars were printed with both screening methods. The conventional screening was elliptical 60 lines per cm screening and the stochastic was Staccato 35, in which the average dot size was 35 μm. The Staccato screening was done with the Creo method. With this kind of layout it was possible to see the differences in piling tendency between the screening systems.

***Table 1***. *Paper samples*

| Sample | Grade and pigment content | Origin EU Europe NA North America | Visual rank low = good | Basis weight / $gm^{-2}$ | Thick-ness / µm | Ash content / % |
|---|---|---|---|---|---|---|
| A | **LWC** more clay than carbonate | EU | 4 | 65 | 53 | 37.8 |
| B | **LWC** more carbonate than clay | EU | 4 | 60 | 52 | 34.4 |
| C | **LWC** more clay than other minerals | EU | 1 | 60 | 54 | 30.2 |
| D | **LWC** more clay than carbonate and other minerals | EU | 1 | 65 | 54 | 31.6 |
| E | **LWC** only clay | NA | 3 | 60 | 52 | 27.6 |
| F | **MWC** only clay | NA | 3 | 60 | 83 | 31.8 |
| G | **LWC single coated** more carbonate than clay | EU | 5 | 65 | 51 | 39.4 |
| H | **wood-free double coated** more carbonate than clay | NA | 2 | 70 | 59 | 27.3 |
| I | **MWC single coated** more carbonate than clay | EU | 2 | 80 | 66 | 36.2 |
| J | **wood-free double coated** more carbonate than clay | EU | 2.5 | 70 | 67 | 41.9 |
| K | **wood-free double coated** more carbonate than clay | EU | 1.5 | 90 | 69 | 42.2 |

***Table 2.*** *Test conditions*

| | |
|---|---|
| **Inks** | Commercial North American type inks<br>Commercial European type inks |
| **Ink sequence** | 1st unit: black<br>2nd unit: cyan<br>3rd unit: magenta<br>4th unit: yellow<br>5th unit: only pressure with fountain solution |
| **Fountain solution** | IPA free, N. American type fount, pH 3.9<br>IPA 6 %, European type fount, pH 5.2 |
| **Fount temp** | 10 °C (50 F) for cool conditions<br>17 °C (63 F) for warm conditions (practice often > 25 °C) |
| **Web speed** | 5.6 $ms^{-1}$ (32 000 rph) |
| **Blankets** | Reeves Vulcan Alto Plus |
| **Printing Plates** | Kodak Gold (Didp Gold – positive plates) |
| **Air temperature** | 22 °C (72 F) |
| **Humidity** | 48 RH-% |

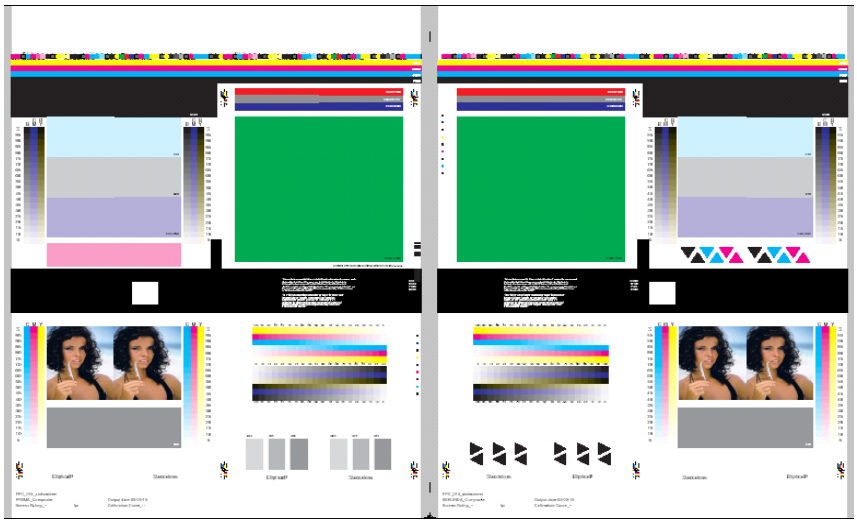

***Figure 2*** *Print form layout for the printing trials.*

The print runnability of the papers with respect to reverse piling was evaluated in the stochastic mid tone region of the first down ink (black) with a non-image area on the opposite face throughout, stochastic screening being shown to be the configuration having the most problems with the press running under N. American conditions. The papers were ranked in order such that the poorest performance paper is placed as 5 and the best performance paper as 1.

## 2. Methods and Results

### 2.1 Impact of Press Parameters

The comparison of North American (NA) with European (EU) press conditions showed the European conditions of lower tack ink and isopropanol (IPA) containing fountain solution to be the less demanding in respect to the reverse piling tendency. However, clearly certain adjustments to the NA system could also be applied to reduce the problem.

One major question that is frequently posed when comparing the two running conditions is: what is the impact of fountain solution pH (NA 3.2, EU 5.9) when carbonate-containing coated papers are used? This is addressed in the following analysis of fountain solution after prolonged running.

#### 2.1.1 Fountain solution analysis

Elemental analysis was made from the fountain solution samples taken each trial point after every 10 000 impressions. Aluminium, calcium and silicon were considered to be of the most interest following the hypothesis of pigment dissolution and especially calcium carbonate leaching. However, it could be shown that the different paper grades did not have an influence in how much calcium is found in the fountain solution, despite the widely varying amounts of carbonate present in the coating formulations. Moreover, approximately the same amount of dissolved calcium was found in the fountain solution of the EU and NA printing conditions virtually independently of the fountain pH. Only about 1-2 $mgdm^{-3}$ more calcium was found in the NA fountain solution system and this amount is considered not to be significant, Figure 3.

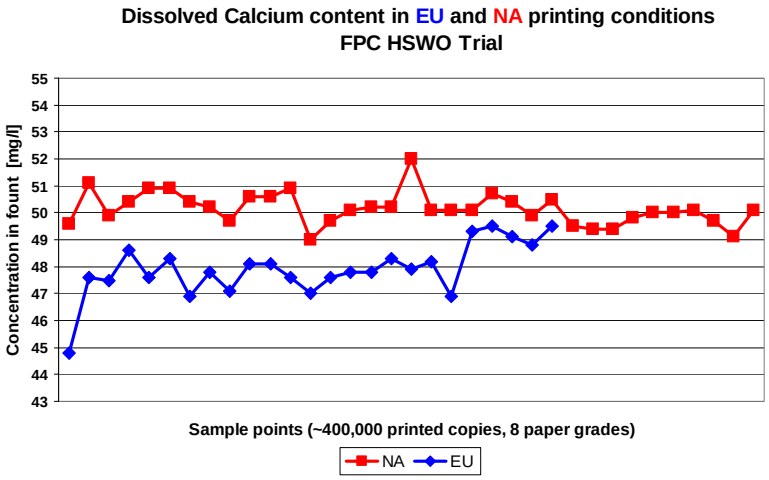


***Figure 3*** *Measured dissolved calcium in the fountain solution supply tank after every 10 000 printed copies for each paper grade comparing North American and European fountain solution types. Clearly both systems reach a similar dynamic equilibrium concentration despite their difference in pH, far away from the static equilibrium saturation level of 475 mg* $Ca^{2+}$ $dm^{-3}$.

## 2.2 Paper-Ink and Paper-Liquid Interactions

### 2.2.1 Ink-Surface Interaction testing

The first interaction analysis of the 11 papers was made using the Ink Surface Interaction Tester (ISIT, SeGan Ltd. Perrose, Lostwithiel, Cornwall PL22 0JJ, U.K.) [Gane *et al*., 1994]. Ink-on-paper tack is measured by a special attachment which consists of a solenoid, a coil spring, a load cell and a contact disc. The separation process using the ISIT, Figure 4, relies on the adhesion of the ink surface to a rubber-like blanket material, resembling that of an offset blanket, which is brought into contact with the ink at a given time after printing. This is achieved by a tack wheel which has the blanket material attached to its surface. The tack wheel is rolled into contact with the ink layer, held stationary and then removed under a controlled force regime (constant rate of change of acceleration). The maximum force required to remove the tack wheel is recorded as the tack force. The sequence is automatically repeated for a predefined number of cycles chosen to span the regions of the tack force under study. The build-up of the tensile force required to achieve each individual separation is recorded with time and can be analysed through specifically designed software. The maximum

level of tensile force at each test point is plotted as measured tack force development with time.

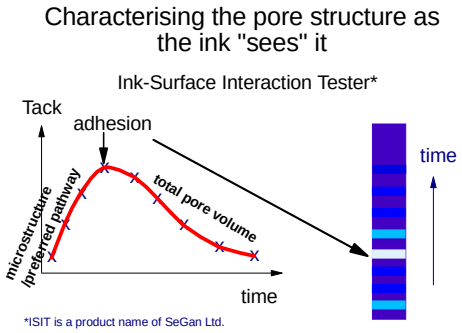


***Figure 4*** *Ink-Surface Interaction Tester: the apparatus and the measurement of ink tack cycle and ink-coating adhesion at maximum tack.*

The curve can be interpreted in three parts: the tack rise, the maximum tack force and the tack decay. The tack rise time, $t_{max}$, is a measure predominantly of the capillary action of the finest pores in the coating, the maximum tack force is a measure of the cohesion in the ink competing against the "affinity" that the ink has for the coating surface. If the tack rise time is short and/or removal of ink occurs at this maximum tack force, i.e. the adhesion of the ink to the coating is poor, it can lead to potential piling problems. Too high a maximum leads to rupture at the weakest point in the paper. The tack decay is a measure of the total pore volume characteristic of the coating "as seen by the ink“. It typically shows the level of coating consolidation that has taken place, for example in calendering or during drying, together with the diffusional properties of ink oils into the polymer network of synthetic binders, such as latex. Often, too fast a fall leads to poor ink curing and a tendency to rub off, and too slow a fall indicates potential for set-off. Furthermore, if the sample shows post-tack adhesion failure, due to too fast a fall, then dry print adhesion is clearly suspect. A further value used to compare samples is derived from this tack fall, the tack decay constant, $\tau_{1/2}$, which is defined as the half height decay time away from the maximum tack, Figure 5.

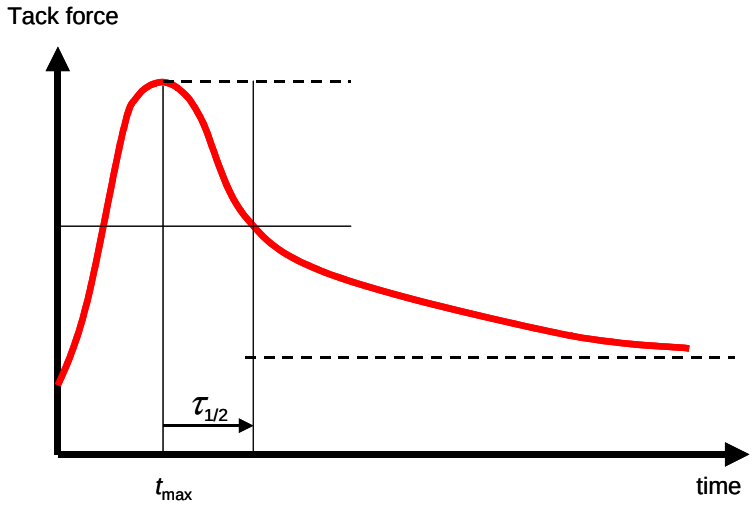


***Figure 5*** *Tack rise time, $t_{max}$, and tack decay constant, $\tau_{1/2}$*

The maximum tack force, $T_{max}$, time to maximum, $t_{max}$, and the tack decay constant, $\tau_{1/2}$, for all the samples are examined, Figure 6 and Figure 7 respectively. The more fine (nano)pores there are present, the faster the tack rise will be and, depending on residual available volume, the tack decay constant may or may not be dependent. When more large pores are present and fewer fine pores then the larger will be the tack decay constant.

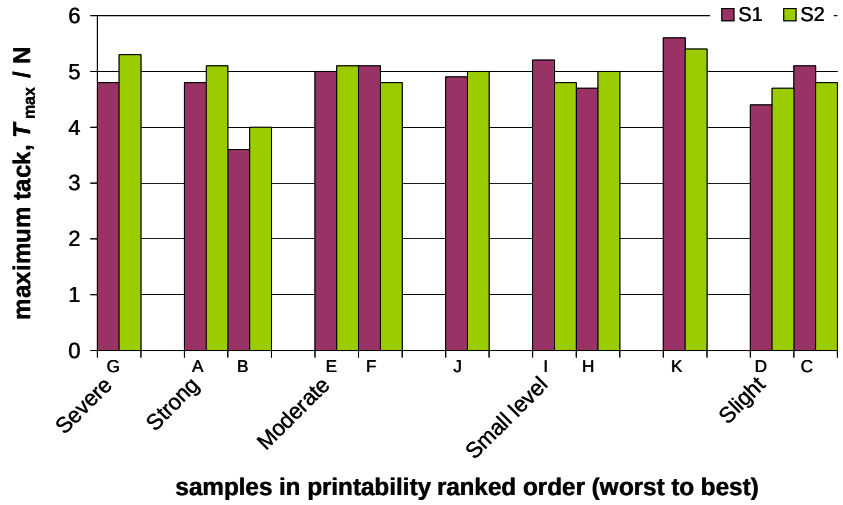


***Figure 6*** *Maximum tack values, $T_{max}$, on the two sides of the paper samples S1 and S2.*

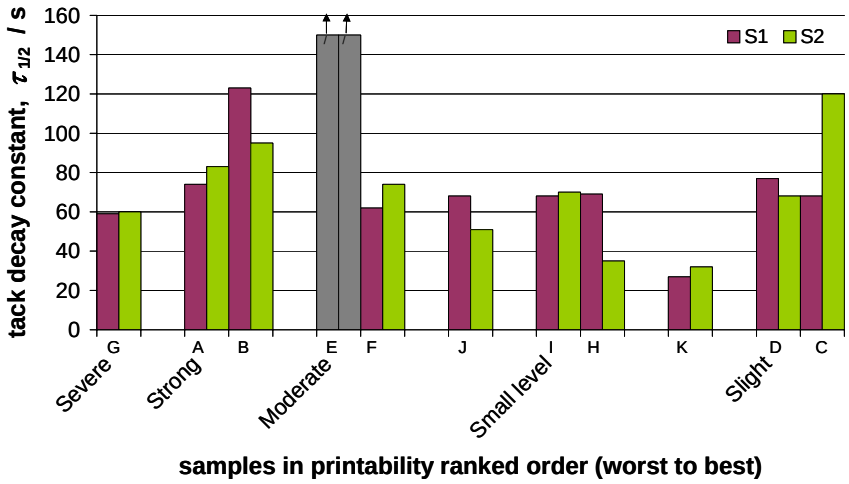


***Figure 7*** *Tack decay constant, $\tau_{1/2}$, on the two sides of the paper samples S1 and S2. Sample E shows non-drying of the ink.*

There do not seem to be any clear trends between $T_{max}$ or $\tau_{1/2}$ in relation to the piling-related runnability of the papers. The case of paper E is unique in the series, in that it is behaving as an uncoated paper in respect to ink tack, i.e. not absorbing ink vehicle to promote complete tackification, except that it does have a smoother surface, higher tack maximum, than would be expected from an uncoated paper. This paper is likely to be coated with a coarse pigment formulation and/or coating coverage is very limited.

In Figure 8, the time to the maximum tack point is plotted against the tack decay constant for measurements on both sides of the papers. Once again paper E is behaving anomalously and more like an uncoated sheet.

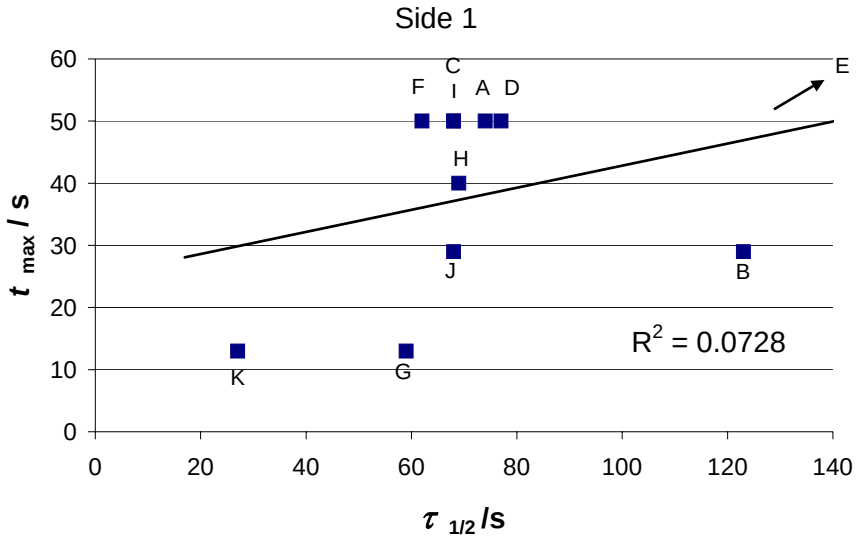

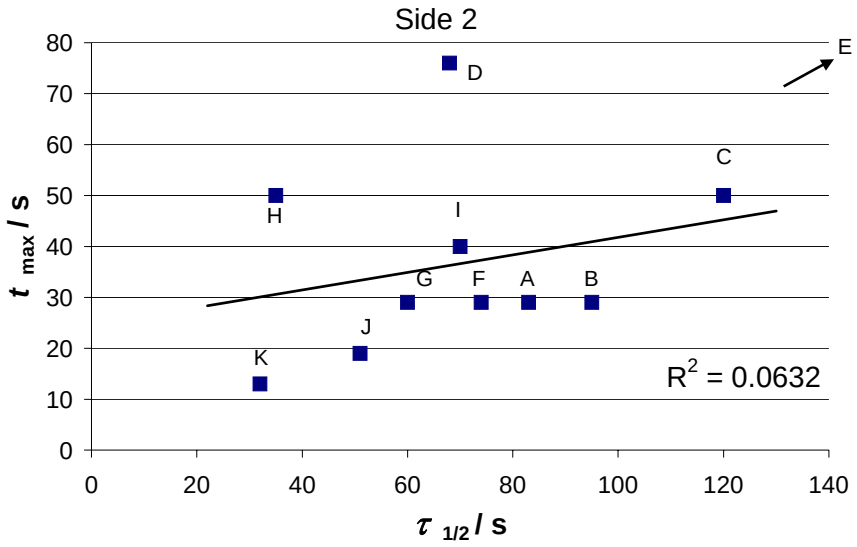


***Figure 8*** *Time to maximum tack, $t_{max}$, plotted against tack decay constant, $\tau_{1/2,}$ for each side of the paper samples*

A number of papers do show strong deviations from side to side. Fitting trend lines to the plots of time to the maximum tack point, $t_{max}$, against tack decay constant, $\tau_{1/2}$, measured on each side of the samples, not surprisingly shows that there is no correlation between the two parameters across the wide range of paper types ($R^2 < 0.1$), though correlation may be present for small variations in each paper construction subset, which suggests that they can be decoupled when considering this series of papers.

A slow tack rise and a relatively fast fall are typical for well controlled ink tack behaviour on a glossy paper. Paper K fulfils these requirements (Figure 8) and indeed lies in the upper rankings based on performance. However, this is clearly not the single controlling criterion for good runnability, i.e. the coating-ink interaction is not the key factor alone. Having stated that these two parameters are not dependent on one another and can be decoupled it is necessary to look at them independently and to determine their influence on the other print materials, including fountain solution, and properties of the press.

### 2.2.2 Porosimetry

Since the results for ink surface interaction alone do not provide correlation with the reverse piling phenomenon, the pore size distribution was investigated to

learn more about the pore volume capacity and likely pore size distribution effects, i.e. the differences between the amount of fine and coarser pore sizes.

For these measurements a strip of the sample is wound into a spiral and held in position with nylon thread to such an outer diameter that it can be placed in the sample holder (penetrometer) without touching the wall. This is to minimise the effects from sample surface contact with itself and with the penetrometer wall during mercury intrusion, which are typical of strongly two-dimensionally biased samples. This procedure prevents the formation of pockets between the sample and the penetrometer that might fail to become intruded at low pressure, and is described in more detail in Ridgway *et al*. [Ridgway and Gane, 2003].

Mercury intrusion measurements were made using a Micromeritics Autopore IV mercury porosimeter. The maximum applied pressure of mercury was 414 MPa, equivalent to a Laplace throat diameter of 0.004 μm (~ nm). The equilibration time at each of the increasing applied pressures of mercury was set to 60 seconds. It is vital that the mercury intrusion measurements be corrected for the compression of mercury, expansion of the penetrometer and compressibility of the solid phase of the sample. This was performed conveniently using the software Pore-Comp (a software program developed by the Environmental and Fluids Modelling Group, University of Plymouth, PL4 8AA, U.K.) [Gane *et al*., 1996].

There are often (irreproducible) differences for a given sample at equivalent Laplace diameters greater than 10 μm, which are generally attributable to the occlusion effect due to the irregularity of surface fibres, as described in a previous publication [Ridgway and Gane, 2003]. The data have therefore been truncated at 10 μm. This means that the total porosity cannot be evaluated, rather the relative porosity in those pores with an equivalent Laplace diameter < 10 μm is derivable by direct comparison of the truncated curves. Figure 9 shows the mercury intrusion curves for the 11 paper samples supplied for testing after correction [Gane *et al*., 1996]. The mercury intrusion data show there is a strong bi-modal distribution for all the papers, representing the basepaper and coating interface pores, and the coating structure independently.

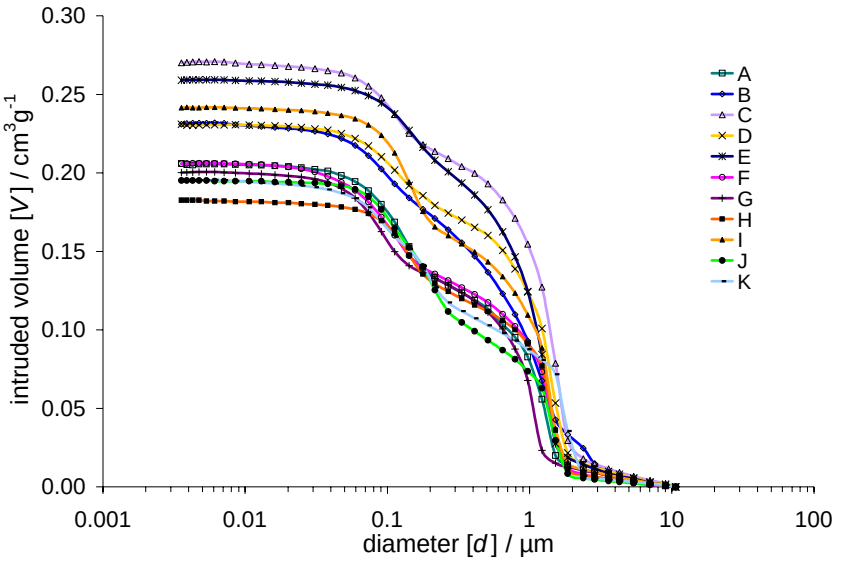


***Figure 9*** *Mercury intrusion curves of the 11 paper samples truncated at 10 µm*

The intruded volumes into the samples over the diameter range 0.004 – 10 µm are summarised in Table 3.

***Table 3****. Total intruded volume into the 11 paper samples*

| **Sample** | **Total intruded volume / $cm^3g^{-1}$** |
|---|---|
| A | 0.21 |
| B | 0.23 |
| C | 0.27 |
| D | 0.23 |
| E | 0.26 |
| F | 0.21 |
| G | 0.20 |
| H | 0.21 |
| I | 0.24 |
| J | 0.20 |
| K | 0.20 |

The mercury intrusion data are indicative of the packing structure and the general fine pore structure of the sheet. By taking the first derivative of the cumulative intrusion curve the pore size distributions based on equivalent Laplace diameter, inevitably including pore-shielding, are revealed. This is shown in Figure 10.

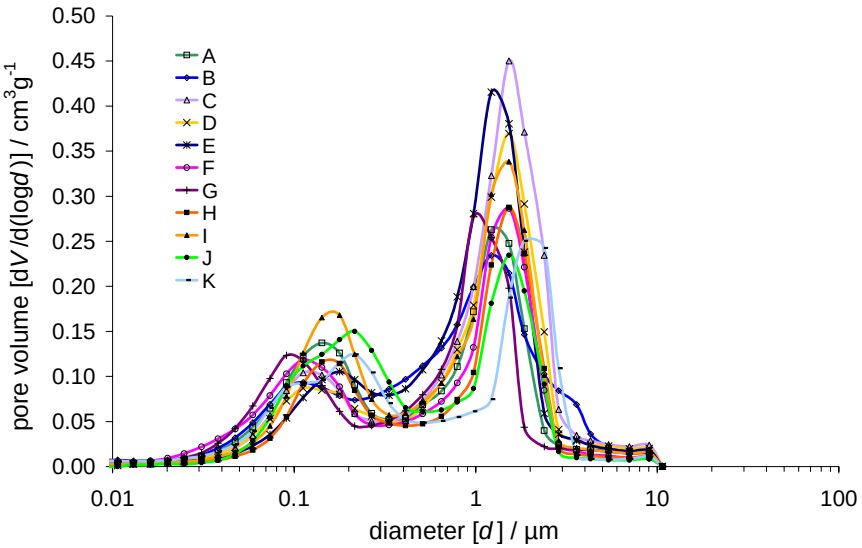


***Figure 10*** *Pore volume distribution of the 11 paper samples*

The fine pores represent the capillarity and combined with the coarse pores represent the permeability and the basepaper structure. Figure 9 shows the fine pore size distributions in more detail.

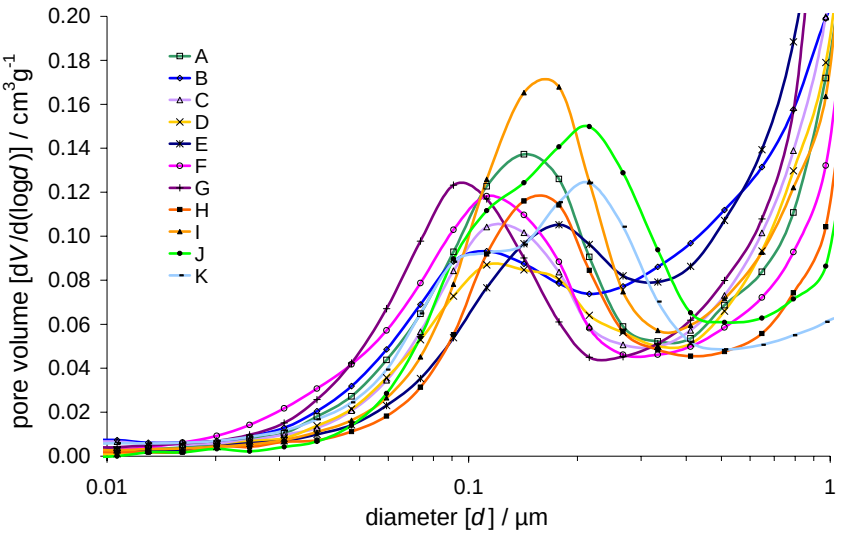


***Figure 11*** *Fine pore volume distribution of the 11 paper samples*

Here in Figure 11 we find the evidence that paper E, unique amongst the set, trends strongly toward a coarse pigment formulation having relatively large coating pores spread in distribution toward the basepaper interface pore region, and thus behaving more like a matt coating structure having a smoothing effect on a surface that otherwise is behaving as an uncoated paper. The multicoated papers J and K show nicely the precoat versus topcoat distributions, inasmuch that the breadth of the secondary peak is increased toward larger pores, i.e. for these two samples the secondary peak is itself bi-modal [Ridgway and Gane, 2003]. Papers F and G have the highest pore volume attributable to the nanopores < 0.1 µm.

The samples with more fine pores lead to a higher capillarity (faster ISIT tack rise) and hence a faster tack rise, $t_{max}$, and possibly tack decay, $\tau_{1/2}$, constant, and this can be seen, for example, with samples F and G. However, if a coating layer is predominantly made up of ultrafine pores, the ability of liquid to flow through the structure (permeability) will be reduced. Since the interaction related to reverse piling appears not to be solely dependent on capillarity differences, we now investigate the permeability of the structures in relation to that capillarity.

### 2.2.3 Permeability in *z* direction of the coated papers

A liquid permeability method is used, which has been described in detail in Ridgway *et al*. [Ridgway *et al*., 2003]. A stack of paper samples (approximately 125 sheets cut to 1.5 x 1.5 $cm^2$) is placed into a mould (Prüfmaschinen AG Giessenstr. 15 CH-8953 Dietikon, Switzerland) having an inner diameter of 30 mm, under a slight overpressure, applied by a suitable light weight to ensure the sheets are lying flat, and resin (Technovit 4000: a product name from Heraeus Kulzer GmbH, Philipp-Reis-Strasse 8/13, D-61273 Wehrheim/Ts, Germany) is poured around it. The quickly rising viscosity of the chosen curing resin results in a penetration of approximately 1 mm locally at the outer boundaries of the sample. This penetration depth is clearly visible because of the opacity change at the edge of the sample and can, therefore, be calibrated. The open area of the porous sample, i.e. that free from resin, is evaluated so that the permeable cross-sectional area can be established. The sample discs are placed in a dish containing the probe liquid in order to saturate the void network of the sample before placing in the apparatus. Hexadecane is used in the experiments, having density $\rho$ = 773 $kgm^{-3}$ and viscosity $\eta$ = 0.0034 $kgm^{-1}s^{-1}$, which is known to fill the entire saturation-available void volume of a pigmented porous structure [Gane *et al*., 2000b], when measured gravimetrically, and largely avoids any interaction with latex or fibres. The sample disc is then placed in a specially constructed pressure cell. The use of the resin to embed the samples allows for rigid clamping and sealing of the sample into the pressure cell chamber. Gas over-pressure is supplied from a nitrogen bottle. The pressure cell is fixed over a microbalance and a PC samples the balance data using specially-developed software (obtainable on request from Dr. C. J. Ridgway, Omya Development AG, CH 4665 Oftringen, Switzerland). A drop captor device is needed in the base of the cell to guide the permeated liquid drops to the outlet. An important point of practical technique is that the whole chamber below the position of the sample has to be pre-wetted with the liquid so that each drop leaving the sample causes a drop to fall into the sampling dish. Once these precautions are taken the continuity of flow is ensured.

The continuous flow can be expressed in terms of the Darcy permeability constant, *k*, as

$$\frac{\mathrm{d}V(t)}{\mathrm{d}t} = \frac{-kA\Delta P}{\eta l} \tag{1}$$

where $\mathrm{d}V(t)/\mathrm{d}t$ is defined as the flux or volume flow rate across an area, $A$, $\Delta P$ is the applied pressure difference across the sample, $\eta$ is the viscosity of the liquid and $l$ is the length of the sample, in this case calculated as the number of sheets multiplied by the sheet caliper.

The permeability is dominated by the coating layer(s) when the coating coverage is complete, and dominated by the gaps in the coating and the basepaper when the coverage is poor, Figure 12.

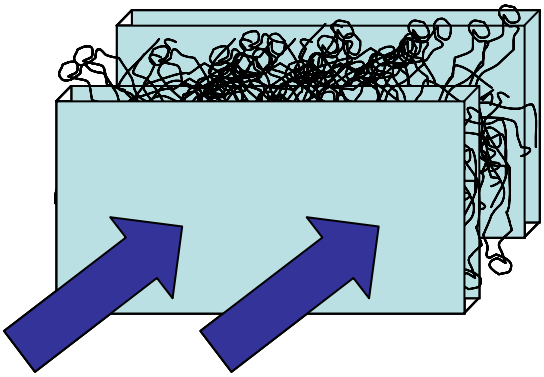


***Figure 12*** *Determining the effects of coating and basepaper on the transplanar permeability*

These experimentally measured liquid permeability values are compared to the Bendtsen air permeability values of these papers [often mistakenly interpreted as "porosity", i.e. it is the flow through the paper and not a quantitative value of the pore space within the paper]. Figure 13 shows these values plotted together with the measured liquid permeability values. The two measurements give similar trends although there is a big scatter with one particular outlier, paper B. Deviation between the two methods signifies a dominant role of the coating coverage - air finds it very difficult to get through a coating and compresses strongly, whereas liquid does not compress. This illustrates that the air permeability is best used for uncoated or only lightly coated papers and less so for heavy weight coated grades.

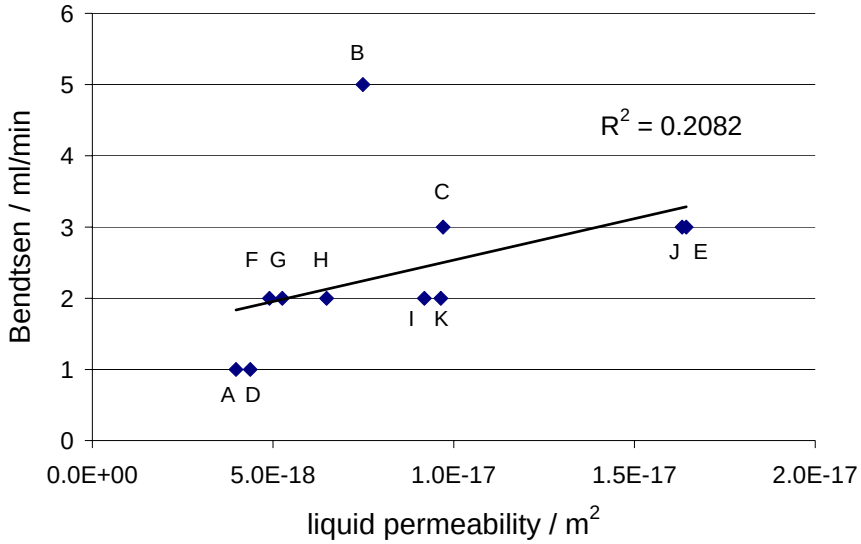


***Figure 13*** *Liquid permeation results in comparison to the more usual air permeability test*

There are frequently geographical differences in respect to basepaper permeability, for example, NA basepapers are seen to be generally more permeable than EU basepapers. When coated, the papers still tend to reflect this property, despite the use of higher levels of clay on NA papers, due to the fact that access to the basepaper in the case of LWC coatings is still a given, resulting from the limitations in coverage, exacerbated in that NA papers also generally have less coating.

Given that the permeability values strongly depend on coverage, the effects of permeability linked primarily to coating structure can only be deduced from these direct permeation measurements in the case of heavily coated papers. Due to this limitation a further step is now taken in which the measured pore structure of the coating is used to model the permeability of the coatings alone.

### 2.2.4 Modelling the Coating Pore Structure

A network computer model, which simulates the void-space structure of porous material, is used to model the structures of the coatings alone to determine the permeability values directly associated with the coating. The model has been employed previously to illustrate structures of a wide range of

porous materials including sandstones [Matthews *et al*., 1996], medicinal tablets [Ridgway *et al*., 1997], soil [Peat *et al*., 2000] and paper coatings [Ridgway *et al*., 2001, Schoelkopf *et al*., 2000]. It uses a unit cell with 1 000 cubic pores in a 10x10x10 array, connected by up to 3 000 throats, i.e. one connected to each cube face, that are either cylindrical or double conical [Ridgway *et al*., 2001] according to the prevailing geometry of the sample material. The structures are optimised such that the simulated intrusion curves match as closely as possible the experimental mercury intrusion curves, and the experimental porosity is accurately reproduced. The model provides not only a structure that eliminates the effects of pore shielding, by considering the porosity in combination with the given Laplace pressures, but also delivers a representative connectivity.

The simulated intrusion curves match closely the experimental mercury intrusion curves, as exemplified in Figure 14, and the experimental porosity is accurately reproduced. The porosities of the coatings were calculated by taking the approximation of the weight proportion of the total pore volume of the sample as related to the ash content, and can be seen in Figure 15. The unit cell for sample J is shown as an example in Figure 16.

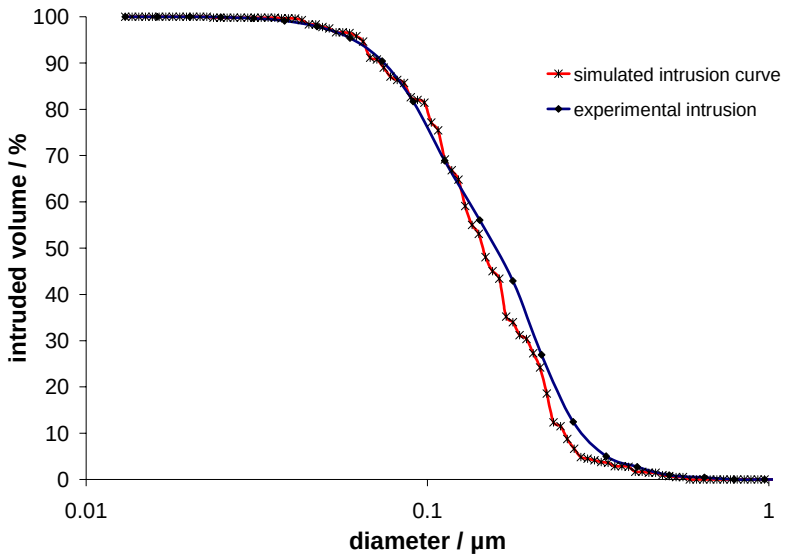


***Figure 14*** *Simulated and experimental mercury intrusion curves for the coating fraction in sample J.*

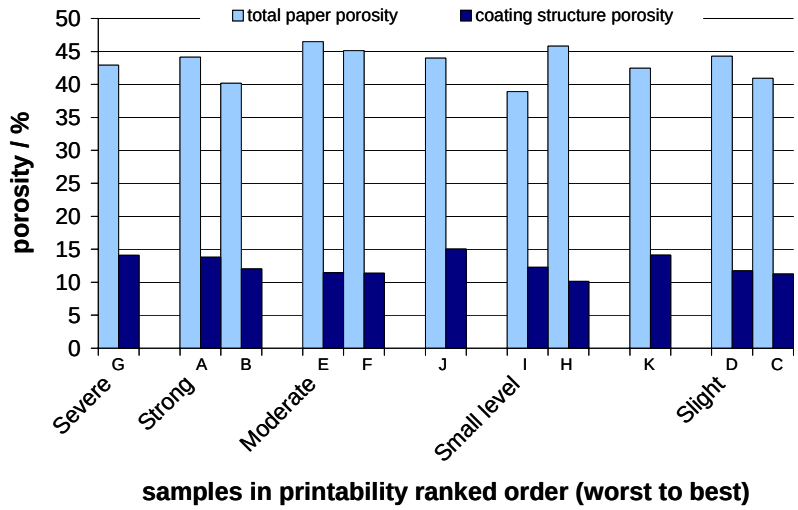


***Figure 15*** *Porosity values of the total paper and of the coating structure alone – samples ranked from bad to good in respect of reverse piling*

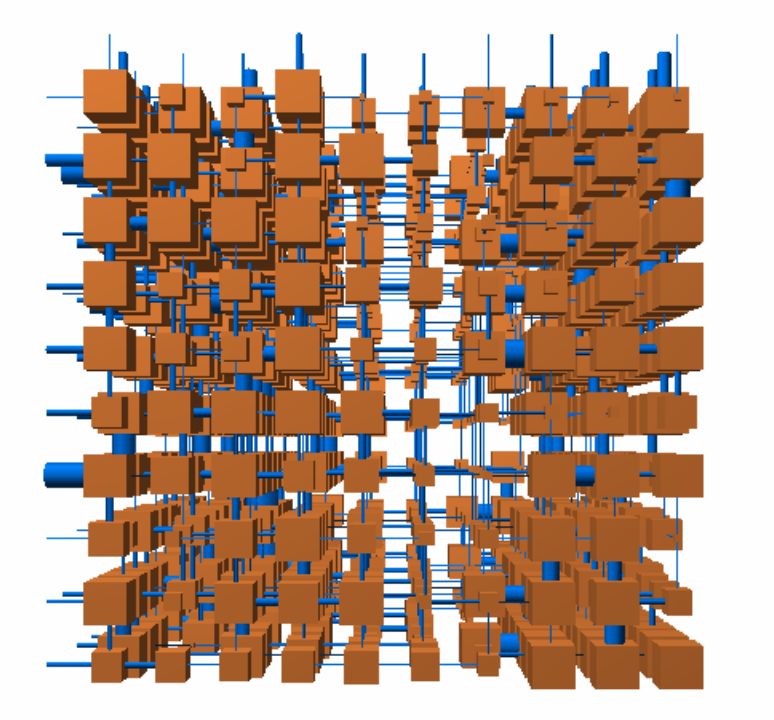

***Figure 16*** *Simulated network structure using cylindrical throats for the coating structure of sample J, unit cell size = 17.96 µm.*

In this case of paper J, as just one example, it is clear to see that the connectivity and throat sizes in Figure 16 are limited, and so one can suspect that the permeability of the coating layer will be lower than suggested by the direct measurement, indicating the effects of reduced coverage.

### *2.2.4.1 Simulated Permeability*

The continuous flow, or permeability, can be expressed as described previously in terms of the Darcy permeability constant, $k$, using Darcy's Law, [Darcy, 1856] [1].

The laminar flow resulting in a parabolic velocity distribution within a liquid volume $V$, in time $t$, for a horizontal circular tube of length $l$, radius $r$, containing a fluid of viscosity $\eta$, flowing under a differential pressure $\Delta P$, is expressed via the Poiseuille equation as:

$$\frac{\mathrm{d}V}{\mathrm{d}t} = \frac{\pi r^4 \Delta P}{8\eta l} \tag{2}$$

where the term $r^4/l$ corresponds to the volumetric flow capacity $\Xi$. In using the Poiseuille equation, it should be recognised that it is only a first approximation to the resistive flow of a feature within the network.

Now it is assumed that Poiseuille flow occurs across the whole cell:

$$\left(\frac{\mathrm{d}V}{\mathrm{d}t}\right)_{\text{cell}} = -\frac{\pi}{8\eta}\,\underset{\text{cell}}{\Omega}\left(\Xi_{\text{arcs}}\right)\Delta P_{\text{cell}} \tag{3}$$

where $\underset{\text{cell}}{\Omega}$ is an averaging operator over the whole unit cell, as described in the work of [Matthews *et al*., 1993] operating on the flow capacities of the arcs ($\Xi_{\text{arcs}}$) in which an arc represents a pore-throat-pore pathway between nodes sited at the centre of each pore. Each arc in the flow network is the flow channel between adjacent nodes, positioned at the centre of each pore. It generates a term which is related to the effective Poiseuillean capacity of the cell for flow in the $-z$ direction (from the top to the bottom face), and in the $\pm x$ and $\pm y$ direction. Flow, however, is not allowed in the $+z$ direction, thereby applying an implicit positive pressure gradient with respect to $z$. A network analysis approach to this problem supplies a term $\underset{\text{cell}}{\Omega}(\Xi_{\text{arcs}})$ as the maximal flow capacity through the network of pores and throats. It is calculated by means of the 'Dinic' network analysis algorithm [Matthews *et al*., 1993]. There is an overall conservation of flow, so that the entire volume of fluid entering the top of the unit cell emerges at the bottom, with no build-up through the network. The value obtained, as the maximal flow, is an average of the capacity values over only those channels found to carry flow.

The combination of the Poiseuille equation, (3), with the Darcy equation, (1), results in an expression for the absolute permeability independent of the pressure gradient imposed on the sample:

$$k = \frac{\pi}{8}\,\underset{\text{cell}}{\Omega}\left(\Xi_{\text{arcs}}\right)\frac{l_{\text{cell}}}{A_{\text{cell}}} \tag{4}$$

The simulated permeabilities, representing the coating alone, are compared with the experimentally measured permeabilities, which represent the paper sample as a whole, i.e. coating and basepaper, in Figure 17.

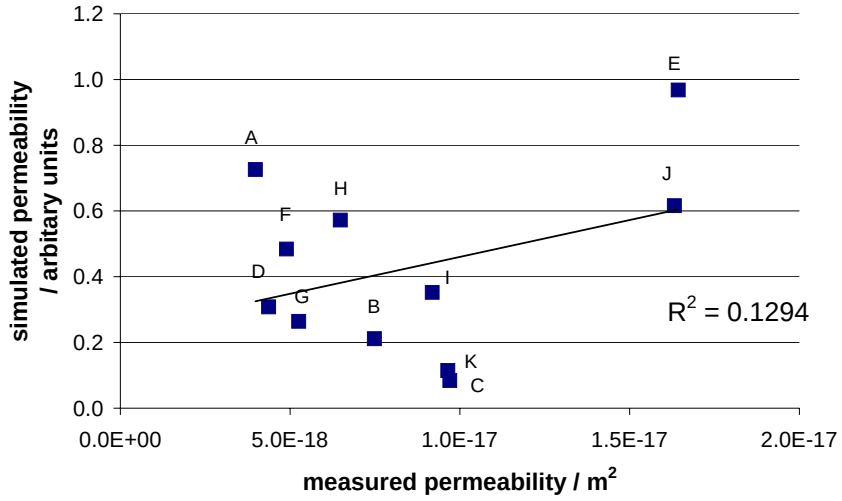


***Figure 17*** *Simulated permeability of coating alone and experimental permeabilities of the coating and basepaper composite*

Samples A, C, E and K stand out as points having big differences between the coating permeability and the permeability of the composite (Figure 17). Sample K is a multicoated product, whereas samples A and C are light weight products. It may be concluded that the differences shown by A and C, in respect to coating permeability, reflect their differences in coating formulation – the clay rich sample C having the lower coating permeability, as would be expected. Sample A on the other hand shows a much higher simulated coating permeability in relation to the measured permeability including basepaper. In this case the permeability of the paper is clearly limited by the basepaper. It can thus be deduced that these samples show relatively poor coating coverage (not surprisingly since they are LWC papers) since their measured permeability is related more to the basepapers than to the coatings. The deviation for sample K, on the other hand, reflects the strong influence of the thicker combined coating layers. Paper E has a highly permeable light weight coating in combination with a relatively permeable basepaper.

The permeability is controlled by the larger pores in the structure as long as they are connected throughout the structure. The permeability, therefore, should be greater the lower the fine pore volume and the greater the larger

pore volume. The volume of fine pores less than 0.1 µm was calculated from the porosimetry measurement, Figure 18. The proportion of < 0.1 µm pores is responsible for the high capillary action pores which "hold on" to liquids and don't let them pass into the basepaper.

Paper C, as discussed above, has a particularly low coating permeability and, as we see, a rather low level of ultrafine pores, Figure 18, though the composite structure with the basepaper included has a higher measured permeability, stressing the strong role of the basepaper in this case. Combining these factors seems to have resulted in the best runnability performance, certainly amongst the light weight papers, though it must be recognised according to the ISIT curve that the reduced volume of ultrafine pores does lead to a slower initial tack response as expected. On the other hand, the isolation of the basepaper by multicoated layers, when present, such as for papers H, J and K, or when heavy coat weight is used, as for paper I, means that the interactions are likely to be overwhelmingly coating dominated, and when sufficient volume is present in such coatings the role of the basepaper is less important.

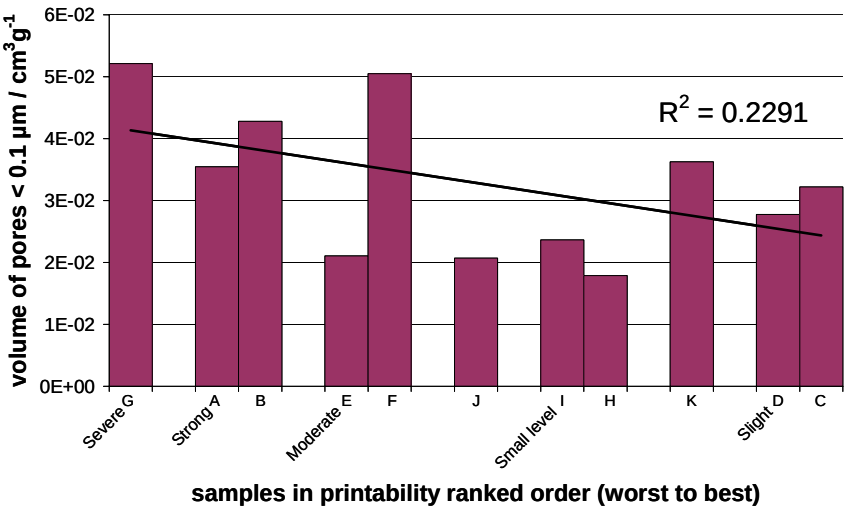


***Figure 18*** *Fine pore volume < 0.1 µm trends weakly with piling tendency: $R^2$ value increases slightly to 0.34 with the exclusion of paper E.*

The additional information we have gained from the comparative permeability analysis now gives us an indication of the parameters requiring detailed investigation, i.e. amount of ultrafine pores, coating permeability and

composite permeability in relation to the absorption power of the basepaper. Hence, the role of basepaper now receives focus so that the composite effect can be more completely elaborated.

### 2.2.5 Absorption by Wicking (length direction)

The accessible porous volume of paper can be measured by absorbing liquid, such as, hexadecane, which, as described in the permeability section, is known to fill the entire saturation-available void volume of a pigmented porous structure [Gane *et al*., 2000b]. By using this alkane, interaction with latex and with fibres, which occurs as a component of many coatings and paper stock respectively, is largely avoided. A number of paper tests that are based on oil absorption make the same assumption [TAPPI Press, 1998].

The method adopts the geometry of wicking of liquid into the *xy* (machine or cross-machine) directions, i.e. length-wise into the paper. These samples were measured for consistency in the machine direction. The sample is hung, dipping into a dish of liquid in a wicking configuration with its planar surface held vertically. The weight loss from the dish is continually recorded in a draught-free environment. This method is descibed in detail in Schoelkopf *et al*. [Schoelkopf *et al*., 2000]. The absorption curves during liquid uptake can be expressed as a linear relationship between the linear flux $V(t)/A$ and $\sqrt{t}$, the gradient of which is

$$\frac{\mathrm{d}(V(t)/A)}{\mathrm{d}\sqrt{t}} = \frac{\mathrm{d}((m(t)/\rho)/A)}{\mathrm{d}\sqrt{t}} \tag{5}$$

where $m(t)$ is the mass uptake at time $t$, as defined by a volume $V(t)$ of fluid of density $\rho$. The data are normalised to the cross-sectional area of the sample, $A$ (an unknown parameter if water were being used due to reaction with fibres), such that the data become $V(t)/A$, the volume absorbed per unit cross-sectional area of the sample. The gradient can be obtained directly from the plotted data by a linear regression analysis. An example of the absorption rate gradient for a paper sample is shown in Figure 19, which shows the mass loss from the liquid source, the negative slope relates to the liquid being lost from the reservoir, i.e. that being absorbed by the paper. This property is not only dependent on capillarity but also on sheet permeability. The gradient of the data gives an absorption rate of the fluid uptake.

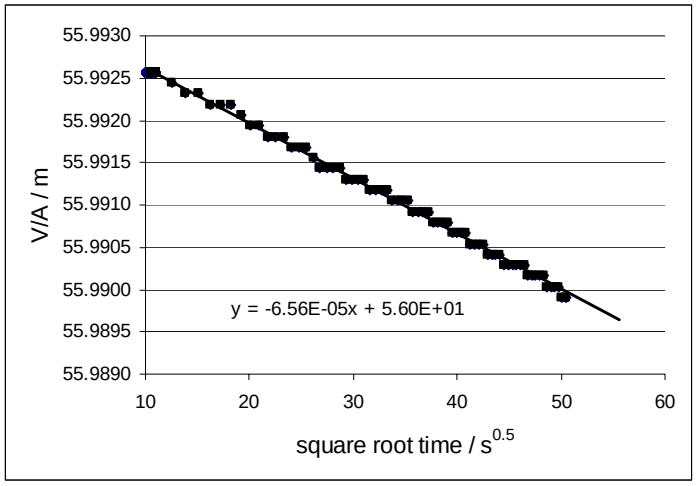


***Figure 19*** *An example of the absorption rate gradient during wicking*

This measurement is dominated by the basepaper (in volume terms), Figure 20, and so gives a measure of absorption rate and capacity of basepaper underlying the coating.

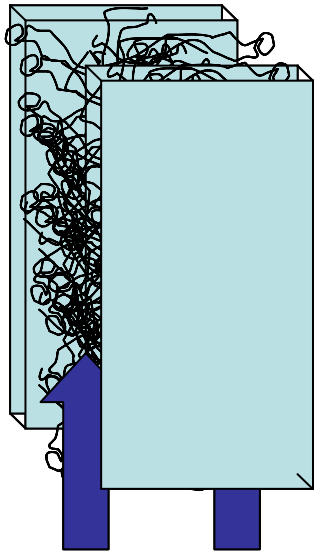

Wicking (basepaper dominated)

***Figure 20*** *Determining the effects of basepaper absorption by wicking*

Figure 21 shows the absorption rates of the hexadecane uptake into the papers calculated as the linear gradient of the volume uptake per unit cross-sectional area plotted against the square root of time. The absorption rates are plotted against the ranking order of the samples.

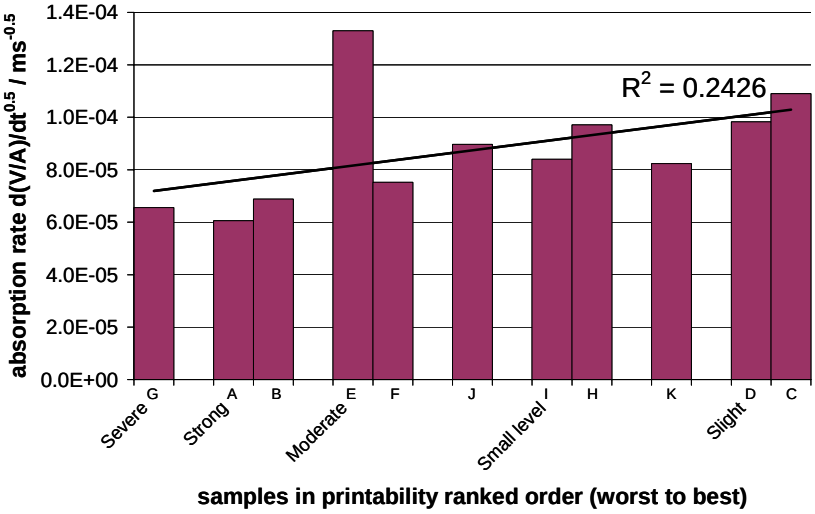


***Figure 21*** *Absorption rate of hexadecane into the paper samples correlates weakly (apart from paper E) with improved piling resistance*

Once again we see the anomalous behaviour of paper E. If this paper is removed from the series then we see a strong correlation with basepaper absorbency, and in general we can say that for most coatings, the basepaper plays a very important role.

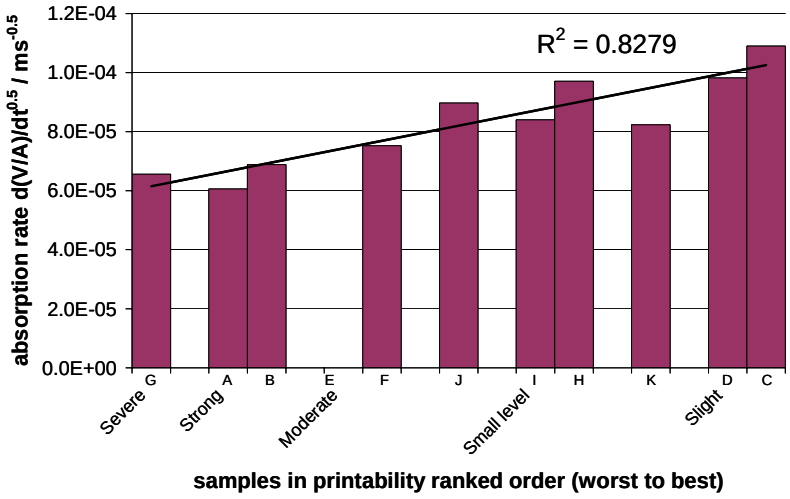


***Figure 22*** *Absorption rate of hexadecane into the paper samples (predominantly basepaper absorbency) correlates strongly with improved piling resistance when paper E is excluded*

As seen, with the exception of paper E, there is clearly a trend showing that a higher absorption rate leads to a better runnability of the paper, i.e. the absorption in the *xy* wicking plane, dominated by the basepaper absorption properties is an important optimisable parameter. Paper E is suspected to have an unsized basepaper, and so the unusually high basepaper wicking in the *xy* direction would be expected, and shows us that the role of the coating needs further description.

The absorption rates are proportional to *xy* permeability over longer periods, provided the capillarity can drive absorption, i.e. the faster the absorption is over long time the less the role of capillarity in retaining liquid. This contrasts to the *z* permeability described earlier, which is a measurement of coating and basepaper together, whereas the absorption measurement here is basepaper dominated in volume terms.

## 3. Discussion: Combining the Factors - Correlating with Press Parameter Performance

We see now from Figures 18 and 21 that a good runnability against reverse piling needs a high coating permeability in the case where the coating contains a significant volume of ultrafine pores (as in most modern high bright papers), together with a high basepaper absorption rate. This combination will act to

avoid a saturated surface of the paper while the ink is experiencing high tack forces. Alternatively, the coating may be non-permeable and non-absorbent: not a realistic option amongst modern high brightness papers unless uneconomic amounts of binder are incorporated.

The results show that the biggest problems on the press set-up shown to generate the reverse piling problem occur when the basepaper has low absorption and the coating is non-permeable but with high capillarity, i.e. fast ink setting but not letting liquid such as fountain solution pass through to the basepaper and preventing rapid equilibration of pressure in the printing nip. The basepaper absorption properties are therefore fundamentally important - it should be absorbent. Depending on the basepaper, the coating should be either non-permeable and low in ultrafine pores if the basepaper is highly absorbent or be permeable when ultrafine pores are present to allow the basepaper volume to be accessed - meaning not having only fine pores, particularly on non-absorbent bases, but a proportion of larger coating pores to allow permeability for liquids to reach the basepaper. This combination is vitally important in the case of light weight papers, where the pore volume in the coating is limited.

Fountain solutions formulated without IPA are frequently less viscous. Furthermore, if the temperature of the fountain solution is higher, so its viscosity will be reduced even more. The basepaper is insulating, so it stays cooler through the press. The coating, however, warms rapidly [Gane *et al*., 2006] and this moves the behaviour into a regime of highly absorbing coating and slow wicking basepaper. Thus, combining a low viscosity fountain solution on a hot press is likely to flood the coating structure. This analysis once again also links in well with the negative effect if the basepaper fails to absorb, as the flow of fountain solution around the laid down ink in the last nip increases. Additionally, both the emulsifying capacity of the ink will decrease generally as a function of reduced fountain viscosity and the sterically dispersed ink pigment may also suffer thermal destabilisation as temperature rises, each effect, either separately or combined, leading once again to the support of the hypothesis of an unstable ink-fountain solution relationship underlying the phenomenon.

The effect of a flooded paper surface, or flooded body of the paper entering a pressure zone, will be to form a thin film effect next to the blanket. It is known that a thin liquid film between two parallel surfaces generates an enormously high force resisting separation, [Poivet *et al*., 2003]. If this thin film forms in the region of the mid tone print, supplied by copious volumes of fountain solution applied at the previous non-image stations both front and back, after the ink has become strongly tackified by capillary action of the coating, the separation forces generated are suspected to lead to ink-coating adhesion failure, particularly when the coating resists pressure equilibration through to the basepaper.

The phenomenon, best described as hydraulic coupling of the blanket and ink via a layer of fountain solution forced above, and/or under the print, is described using the novel term, "aquapiling", and illustrated graphically in Figure 23.

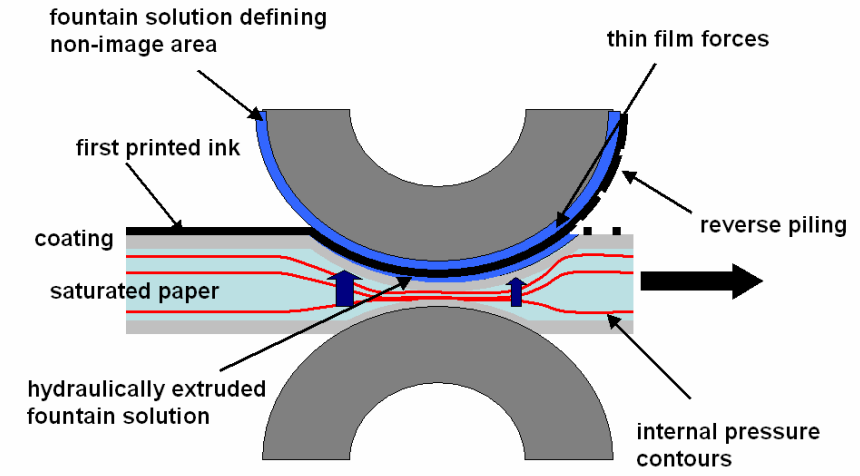


***Figure 23*** *Mechanism of aquapiling in the printing nip. The diagram illustrates the action in the area of a one-side printed dot as the paper moves from left to right in a subsequent printing nip.*

To get at the relative importance of the combined effects, i.e. coating capillarity and permeability, and basepaper absorption potential, each with their relatively low $R^2$ correlation factors due to outlier points in each response separately, Figure 18 and Figure 21, respectively, a function was generated using the parameters of wicking rate in the dipping experiment, raised to the power $a$, multiplied by the volume of pores < 0.1 µm, raised to the power $b$, where $a$ and $b$ are adjusted to make the product approximately constant. By plotting the log of each of the parameters against each other it can be shown that the gradient is negative and that $a/b$ is 1.07, showing that both effects are very important and can either support each other or have a cancelling property, Figure 24, but that the coating plays the slightly dominant role when viewing the complete series of papers. It also supports the obvious case of heavy weight coated papers in that the relevance of the coating is of course even greater, but for lightweight papers with porous and permeable coatings, maintaining the basepaper absorbency is the key parameter that can be used to prevent reverse piling.

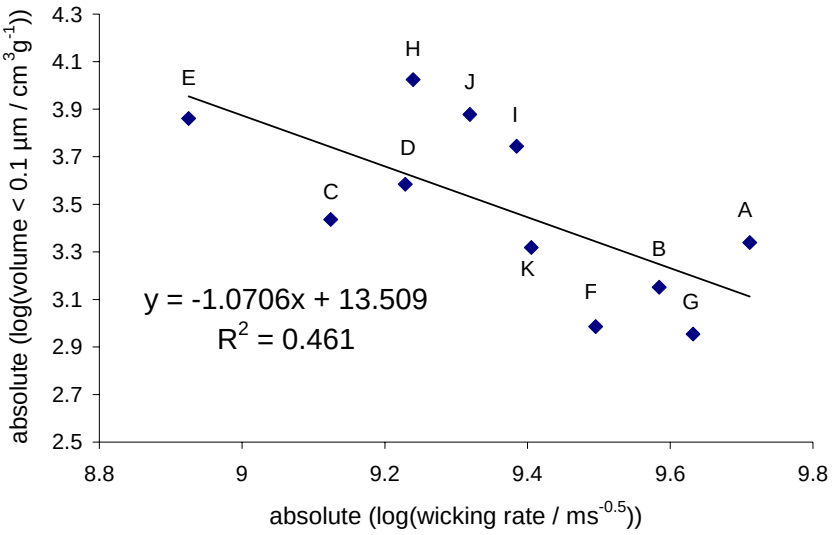


***Figure 24*** *The relationship between wicking rate in the dipping experiment, raised to the power a, and the volume of pores < 0.1 µm, raised to the power b.*

We can now explain the anomalies in the previous weak correlations by incorporating coating permeability when we combine the two anti-correlating properties permeability with and without capillarity, together with basepaper absorbency, under the expression

$$\text{reverse piling} \propto \frac{[\text{coating permeability NAND capillarity}]}{[\text{basepaper absorbency}]\,[\text{coating capillarity AND permeability}]} \quad (6)$$

where "AND" and "NAND" are Boolean operators referring to "combined with" and "not combined with", respectively.

If the coating is too permeable and its capillarity low combined with a basepaper that is wicking strongly then the fountain solution flows too easily around the sheet and can re-surface from deeper in the base paper under pressure. This is best illustrated by paper E which has high basepaper absorption potential and a high coating permeability with a low level of fine pores, i.e. low capillarity. The case E, not being a particularly good paper, therefore, resolves itself in the ranking despite the basepaper wicking by realising that the coating is of particularly low capillarity. If the basepaper has extremely high wicking, and the coating has low capillarity, the absorption in practice is brought under control by reducing the coating permeability. This is a practical solution as illustrated by

paper C. The interesting role of permeability of the coating is crucial as to whether it is present together with capillarity = good in moderation, or without capillarity = bad.

The same argument vice versa applies for the anomalous case in the permeability/capillarity ranking. The permeability is the rate at which fluid reaches the basepaper, E and J being the exceptions being high showing very little coating effect on reducing permeability.

## 4. Conclusions

The substrate effects relating to reverse piling in the case of a one-side single colour printed image on a multicolour offset press have been analysed. No direct trend between the effect of either paper weight or coating pigment formulation alone could be drawn. The results of a range of tests, including wicking of liquid into the paper in the planar machine direction, dominated by the basepaper absorption properties, cross planar air and liquid permeability, dominated by the coating structure and coverage, ink tack behaviour using the ISIT ink-on-paper tack method, mercury intrusion porosimetry and modelling of the coating layer using a network simulator (Pore-Cor) to determine its permeability separate from that of the basepaper, have been used to support a theory concerning the interaction of the repeated application of excess surface fountain solution and the first laid-down ink. It is shown that the problem is linked to the combination of two main properties: low absorption potential by the basepaper matched by a lack of permeability of the coating in the case and only in the case when capillary forces in the coating are high, as determined by a high proportion of ultrafine pores (< 0.1 μm) which is typical of modern high brightness coated papers. The case is illustrated particularly where a highly absorbing basepaper can either assist when the coating layer is particularly impermeable, or be damaging when the coating is very permeable without high capillarity. Additionally, the negative effect of increasing the temperature of the fountain solution, i.e. reducing its viscosity, by reducing the cooling, further supported the hypothesis, in that the more thermally conducting coating layer is suspected to have run at a higher temperature than that of the more insulating basepaper, rendering a reduction in the relative absorption properties of the basepaper in comparison to the effectively increased coating permeability as the fountain solution met the cooler basepaper.

The destabilising effect of reduced emulsion capacity in some ink-fountain solution combinations and the allied potential for thermal destabilisation of sterically dispersed ink pigment in the presence of warm fountain solution are considered to be combinatory factors to the aquapiling phenomenon described,

which, when combined with the substrate parameters identified in this work, lead to the problem of reverse piling.

**5. Literature**


Concannon, P.W. and Wilson, L.A., (1992), *"A Method for Measuring Tack Build of Offset Printing Ink on Coated Paper", TAGA Conference Proceedings, Vancouver*

Darcy, H., (1856), *"Les Fontaines Publiques de la Ville de Dijon", Appendix - Note D, 559-603.*

Gane, P.A.C., Kettle, J.P., Matthews, G.P. and Ridgway, C.J., (1996), *"Void Space Structure of Compressible Polymer Spheres and Consolidated Calcium Carbonate Paper-Coating Formulations", Industrial and Engineering Chemistry Research, 35(5), 1753-1764.*

Gane, P.A.C., Ridgway, C.J., Schoelkopf, J., and Bousfield, D.W., (2006), *"Heat transfer through calcium carbonate-based coating structures: Observation and model for a thermal fusing process", Tappi International Printing and Graphic Arts Conference, Cincinnati, Tappi Press, Atlanta.*

Gane, P.A.C., Schoelkopf, J., and Matthews, G.P., (2000a), *"Coating imbibition rate studies of offset inks: a novel determination of ink-on-paper viscosity and solids concentration using the ink tack force-time integral.", International Printing and Graphic Arts, Savannah, Tappi Press, Atlanta.*

Gane, P.A.C., Schoelkopf, J., Spielmann, D.C., Matthews, G.P. and Ridgway, C.J., (2000b), *"Fluid Transport into Porous Coating Structures: Some Novel Findings", Tappi Journal, 83(5), 77-78.*

Gane, P.A.C., Seyler, E., and Swan, A., (1994), *"Some novel aspects of ink/paper Interaction in offset printing", International Printing and Graphic Arts Conference, Halifax, Nova Scotia, Tappi Press, Atlanta.*

Matthews, G.P., Moss, A.K., Spearing, M.C. and Voland, F., (1993), *"Network Calculation of Mercury Intrusion and Absolute Permeability in Sandstone and Other Porous Media", Powder Technology, (76), 95-107.*

Matthews, G.P., Ridgway, C.J. and Small, J.S., (1996), *"Modelling of Simulated Clay Precipitation Within Reservoir Sandstones", Marine and Petroleum Geology, 13(5), 581-589.*

Peat, D.M.W., Matthews, G.P., Worsfold, P.J. and Jarvis, S.C., (2000), *"Simulation of Water Retention and Hydraulic Conductivity in Soil Using a Three-Dimensional Network", European Journal of Soil Science, (March 2000), 65-79.*

Poivet, S., Nallet, F., Gay, C. and Fabre, P., (2003), *"Cavitation-Induced Force Transition in Confined Viscous Liquids Under Traction", Europhysics Letters, 62, 244-250.*

Ridgway, C.J. and Gane, P.A.C., (2003), *"Bulk Density Measurement and Coating Porosity Calculation for Coated Paper Samples", Nordic Pulp and Paper Research Journal, 18(1), 24-31.*

Ridgway, C.J., Kalela, E. and Gane, P.A.C., (2002), *"Ink-Coating Adhesion: Factors Affecting Deposits on the CIC in 'Satellite' Type CSWO Presses When Using VAC Papers", Journal of Graphic Technology, 1.1, 49-58.*

Ridgway, C.J., Ridgway, K. and Matthews, G.P., (1997), *"Modelling of the Void Space of Tablets Compacted Over a Range of Pressures", Journal of Pharmacy and Pharmacology, 49, 377-383.*

Ridgway, C.J., Schoelkopf, J. and Gane, P.A.C., (2003), *"A New Method for Measuring the Liquid Permeability of Coated and Uncoated Papers and Boards", Nordic Pulp and Paper Research Journal, 18(4), 377-381.*

Ridgway, C.J., Schoelkopf, J., Matthews, G.P., Gane, P.A.C. and James, P.W., (2001), *"The Effects of Void Geometry and Contact Angle on the Absorption of Liquids into Porous Calcium Carbonate Structures", Journal of Colloid and Interface Science, 239(2), 417-431.*

Schoelkopf, J., Ridgway, C.J., Gane, P.A.C., Matthews, G.P. and Spielmann, D.C., (2000), *"Measurement and Network Modeling of Liquid Permeation into Compacted Mineral Blocks", Journal of Colloid and Interface Science, 227(1), 119-131.*

TAPPI Press, "1998-1999 Tappi Test Methods", Tappi Press, Atlanta, (1998).